Biotribology 13 (2018) 23–29

Contents lists available at ScienceDirect

Biotribology

journal homepage: www.elsevier.com/locate/biotri

In Situ Measurements of Contact Dynamics in Speed-dependent Hydrogel Friction

Eric O. McGhee, Angela A. Pitenis, Juan Manuel Urueña, Kyle D. Schulze, Alexander J. McGhee, Christopher S. O'Bryan, Tapomoy Bhattacharjee, Thomas E. Angelini, W. Gregory Sawyer*

Department of Mechanical and Aerospace Engineering, University of Florida, Gainesville, FL 32611, United States

ARTICLE INFO

Keywords:
Hydrogels
Deformation
Contact dynamics
Friction
Plowing
Confocal microscopy

ABSTRACT

The friction behavior of soft, aqueous, biotribological contacts depends on contact geometry, speed, and pressure. Previous efforts to measure the surface profile of soft sliding contacts have been stymied by the matching index of refraction of aqueous materials submerged in water. Here, hydrogel surface deformations were imaged using confocal microscopy to experimentally investigate the contact geometry as a function of sliding speed. *In situ* fluorescence confocal microscopy measurements of the contact deformation during unidirectional friction experiments revealed the existence of a front/back asymmetry that increased with increasing sliding speed. A polyacrylamide hydrogel disk (96.5% water) was polymerized with fluorescent dyes and used as a rotating countersample below a polished glass hemispherical pin (1 mm radius of curvature). All experiments were performed submerged in a dilute (0.7 wt%) suspension of 1 μm red fluorescent microspheres in ultrapure water. Imaging of the contact was performed using a confocal microscope *in situ* with unidirectional sliding at 0.1, 1, 10, and 100 mm/s. The friction coefficient increased monotonically with increasing speed from $\mu \sim 0.04$ at 0.1 mm/s to $\mu \sim 0.20$ at 100 mm/s. All imaging was performed relative to the stationary glass probe under steady-state conditions. The contact line measured by connecting the leading and exiting contact points was nearly perpendicular to the loading direction at 0.1 mm/s sliding speed, but distorted as sliding speed increased. Consistent with the theories of viscoelastic contributions to polymer friction, the tangent of the contact-line angle correlated with friction.

1. Introduction

Aqueous lubrication with soft hydrogels, tissues, cartilage, and biopolymers frequently reveals a friction dependence on sliding speed. A number of different mechanisms have been suggested to explain this dependence, including a hypothesis of viscoelasticity in which a "plowing" component of friction is sensitive to sliding speed. As discussed by Bonnevie et al., the plowing contribution of friction is attributed to the integrated pressure distribution having a component parallel to the sliding vector but in the opposite direction [1]. Bonnevie et al. also discussed that these plowing contributions, "cannot be determined without known pressure distributions". The prevailing theory is that viscoelastic effects lead to an asymmetry in the pressure distributions – viscoelasticity is frequently measured and modeled for cartilage, tissues, and high-water content gels [2–6].

A recent finding using self-mated contacts of identical hydrogel samples (Gemini hydrogels) revealed a surprising speed independence in friction coefficient that spanned over 2 orders of magnitude in sliding speed [7], which was notable as the majority of healthy biological sliding interfaces are in Gemini configurations. This study raised questions as to whether or not *in vivo* biological interfaces experienced speed-dependent friction, or if they were effectively constant friction interfaces. In an effort to tease out the fundamental mechanisms underlying the friction behavior of biological interfaces, high-water content hydrogels have been used as convenient surrogates for *in vitro* studies [7–9]. The optical clarity, tunable mechanical and transport properties through changes in the mesh size (ξ), wide range of water content, and ease of fabrication have made these hydrogels nearly ideal experimental samples for studies of aqueous lubrication. One recent, and perhaps surprising, discovery was that friction coefficient decreased with increasing mesh size, and that this could continue into the regime of superlubricity ($\mu < 0.005$) [9,10]. As elastic modulus falls rapidly as mesh size increases (E proportional to $\xi^{-1/3}$) [11]. These superlubricious hydrogels were almost "slime-like" in their mechanics as elastic modulus falls rapidly with increasing mesh size ($E \sim \xi^{-1/3}$) [11], suggesting that the softest surface gels in bio-lubrication may be

* Corresponding author.
E-mail address: wgsawyer@ufl.edu (W.G. Sawyer).

https://doi.org/10.1016/j.biotri.2017.12.002
Received 13 October 2017; Received in revised form 1 December 2017; Accepted 23 December 2017
Available online 24 December 2017

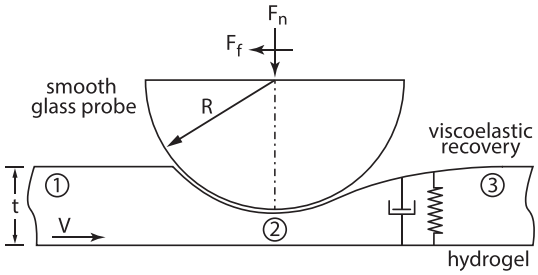

Fig. 1. An illustration of contact showing the modified Winkler foundation model which adds a viscoelastic component to the response of the material undergoing sliding friction. Considering a viscoelastic material undergoing dynamic deformation, three distinct regions of deformation become apparent: (1) the *inlet* region, or leading edge; (2) the *apex* region at the tip of the indenting probe; (3) the *exit* region, or trailing edge. Adapted from Rennie et al. [28].

responsible for the low friction coefficients that rival values found under hydrodynamic lubrication.

Physiological sliding speeds span a wide range from nm/s for cell migration to over 100 mm/s for blinking and joint movements. Gemini hydrogel experiments performed over a range in speed, 30 μm/s to 100 mm/s, revealed a critical transition speed at which friction coefficient rises with increasing sliding speed, and this transition may be related to the polymer relaxation time [8,9]. Speed-dependent friction behavior has also been observed in cartilage systems [12], and the hypothesis for this behavior was a form of viscoelasticity in which fluid depressurization in the cartilage matrix due to fluid exudation in the wake of contact resulted in a time-dependent recovery following deformation. Bonnevie et al. argued that in a contact configuration of a rigid sphere sliding against a flat countersample of cartilage, the trailing half of the contact could not provide meaningful load support and thus only the front half supported the load. This concept was consistent with simulations by Kusche [13] that modeled the sliding of a probe over an indented viscoelastic half-space at sufficiently high sliding speeds (Fig. 1).

The hypothesis of a viscoelastic effect on friction for soft biomaterials is essentially one of leading/trailing edge contact asymmetry. Earlier studies have investigated the deformed surface profile of flat transparent elastomers loaded under a clean glass hemispherical probe and used Newton's rings to determine contact area in static and dynamic conditions [14]. Barquins and Courtel directly observed an asymmetric contact patch of a soft elastomer under hemispherical contact develop as sliding speed increased but were unable to image the surface profile. Schulze et al. [15] observed a complex speed-dependent folding and contact patch evolution when sliding soft rubber spheres against smooth glass countersurfaces. Krick et al. and Persson et al. used similar methods under liquid-lubricated conditions to resolve changes in contact area during the sliding of soft hemispherical probes against smooth glass surfaces [16,17]. The insight provided by these experiments for understanding elastomer tribology suggests that direct visualization of the contact patch and adjacent regions during sliding may also be necessary to elucidate the mechanisms of speed-dependent friction at hydrogel surfaces. Further, direct observations and measurements of hydrogel surface profiles during loading and sliding may reveal insights into the nature of biological sliding contacts, such as those found in cartilaginous joints or the cornea-eyelid interface.

Here we describe *in situ* experiments measuring the surface profile of a deforming hydrogel sample sliding against a spherical glass probe. These experiments were performed and imaged using 3D confocal laser-scanning microscopy under a condition of dynamic equilibrium where fluorescent particle dispersions were used to delineate the borders between the hydrogel surface, water, and the glass probe. Imaging was performed relative to the stationary spherical probe that was loaded into contact with a submerged hydrogel countersurface spinning under steady angular speed. The deformation profiles over a range of sliding speeds from 0.1 mm/s to 100 mm/s were analyzed and compared to changes in friction coefficient as a function of sliding speed.

2. Materials and Methods

2.1. Hydrogel Preparation and Characterization

Polyacrylamide (pAAm) hydrogel disks (~10 mm thick) were polymerized at room temperature from a precursor solution, reported as weight-solute per weight-total percentages: 3.75% acrylamide monomer, 0.15% *N,N′*-methylenebisacrylamide cross-linker, 0.15% ammonium persulfate initiator, 0.15% tetramethylethylenediamine catalyst in ultrapure water (18 MΩ). FluoroMax green fluorescent microspheres (5 μm diameter) were included in the precursor composition at 0.002 wt% in solution. To ensure flatness and low surface roughness, disks were cast between two polystyrene culture dishes (Ra ~ 20 nm). After curing, the disk diameter was reduced to 24 mm and equilibrated in ultrapure water for ~5 days prior to experimentation. The elastic modulus of the gel (E~500 Pa) was determined from indentation experiments following the methods in Pitenis et al. [8], except with a hemispherical borosilicate glass probe (1 mm radius of curvature) in this study.

2.2. In Situ Friction Experiments

Unidirectional sliding was performed using a pin-on-disk microtribometer mounted to a confocal laser-scanning inverted microscope (Nikon C2). A double-leaf cantilever (normal stiffness of 148 μN/μm, and lateral stiffness of 69 μN/μm) with two 3 mm capacitive displacement sensors were used in combination to measure normal and lateral forces during contact and sliding. The cantilever was secured below an XY-axis translation stage (OptoSigma TAM-602 high precision linear stages), which was mounted in place of the microscope condenser head. A high-speed piezoelectric rotary stage (Physik Instrumente M-660.55, 4-μrad resolution) was fixed to the microscope stage. The hydrogel disk was placed in a custom dish with an optical window and mounted to the rotary stage. A 17.5 wt% pAAm was polymerized in the free space around the soft sample and thus secured it in place. A hemispherical borosilicate glass probe (1 mm radius of curvature) was attached to the cantilever. During sliding, the hydrogel disk and glass probe were completely submerged in a 0.7 wt% dispersion of FluoroMax red fluorescent microspheres (1 μm diameter) in ultrapure water, to provide an additional image channel to delineate the deformed hydrogel surface.

The experiments described herein were very sensitive to misalignments so accurate measurements of hydrogel surface deformations depended on adequate leveling prior to sliding. The hydrogel disk was leveled with respect to the probe to within ± 20 μN by loading the glass probe into contact with the gel to a normal force of 1 mN, then rotating the disk in 360° increments and performing fine adjustments using three leveling screws on the custom dish. After the leveling procedure, the glass probe was unloaded and the hydrogel disk equilibrated for ~2000 s. A reference surface was established by imaging the undeformed surface of the rotating hydrogel disk at the prescribed constant speed (0.1, 1, 10, or 100 mm/s).

Before and after each set of sliding speed experiments, the hydrogel disk was allowed to equilibrate for ~2000 s before reimaging to confirm a level surface. The glass probe was translated using the XY-axis stage to a new location on the hydrogel and loaded to a normal force of 1 mN. The hydrogel rotated beneath the probe at the prescribed constant speed (0.1, 1, 10, or 100 mm/s) with an 8 mm radius contact path and a contact width of ~1.5 mm, which ensured negligible errors in friction coefficient [18]. The normal force was not controlled during sliding, which allowed free amplitude variations due to potential rate-dependent deformations of the hydrogel surface.

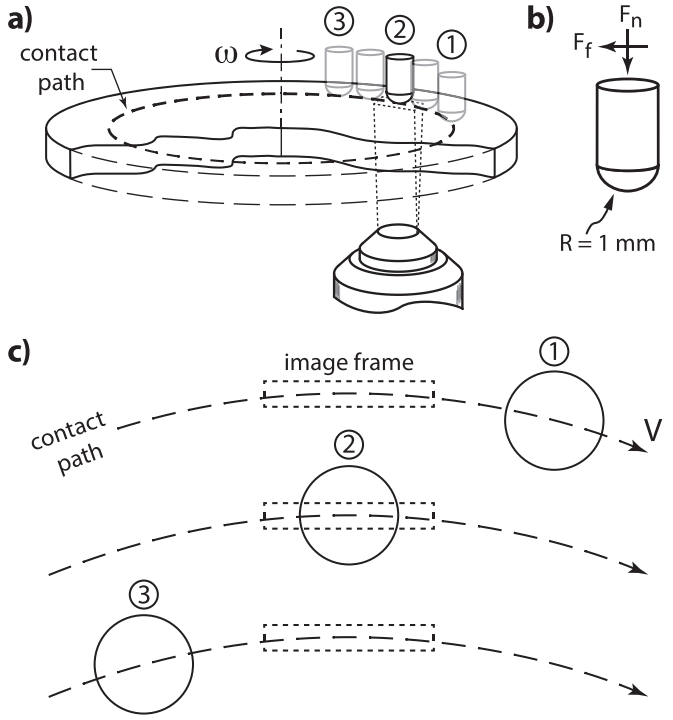

Fig. 2. Schematic of the experimental setup and procedure. (a) The configuration consists of a glass probe (1 mm radius of curvature hemisphere) mounted to a cantilever (not shown), and a rotating hydrogel disk with a contact path radius of 8 mm. The microtribometer is mounted above a confocal laser-scanning microscope which captures surface profile images of the hydrogel disk during sliding. Translated positions of the fixed probe are shown as transparent illustrations. (b) Illustration of glass probe attached to nylon rod. Normal and friction forces are reacted through the rod attached to a cantilever. (c) Multiple translation positions were used to generate composite images to capture the full hydrogel surface deformation to ± 3 contact radii from the probe apex. The probe (circles) is translated along the circumferential contact path (curved dashed line) with respect to the fixed image frame (dashed box). To image the inlet regions (1), the probe is translated along the contact path to the right of the imaging frame, thereby shifting into frame the inlet region. To image the apical region (2), the probe is translated to a position directly above the image frame. Finally, to image the exit regions (3), the probe is translated along the contact path to the left of the image frame, thereby shifting into frame the exit region.

2.3. In Situ Confocal Microscopy and Image Processing

Composite images of contact were created from a series of seven confocal stacks from the inlet to exit regions (Fig. 2a, b) to capture maximum and far-field deformations (out to ± 3 contact radii from the probe centerline) during sliding. These images were generated by translating the probe along the circumferential contact path and taking seven separate confocal stacks of the same height, length, width, and absolute z-position while sliding. One confocal stack was taken for each probe translation. Since image dimensions did not change throughout experiments, this allowed for stitching and direct comparison between images.

Unidirectional confocal laser scanning was conducted at a framerate of 8 fps using a 10 × objective. The green and red fluorescent particles were excited using laser light of wavelengths 488 nm and 561 nm, respectively. Each of the seven stacks per composite image required nearly 180 s due to the acquisition rate of the confocal camera-such laser light exposure diminishes intensity of the fluorescent microspheres. To counteract this bleaching effect, laser intensity was increased incrementally in order to generate approximately the same intensity profile histograms across confocal stacks.

For each individual confocal stack, 164 confocal images were taken vertically through the hydrogel during sliding with a final stack height of 1.1 mm. These stacks were collapsed and flattened into individual X-Z images of dimensions 1.2 mm wide (X) by 1.1 mm tall (Z) using image processing software (Fiji ImageJ) [29]. Individual images were rotated to correct for any misalignments of the hydrogel surface with respect to horizontal, then stitched together into a probe-centered composite of 7.5 mm wide by 1.1 mm tall (Fig. 3a).

During testing, rotational run out, rotational frequency at 10 mm/s, and confocal imaging frequency combined to generate images where the surface could not be accurately distinguished. Due to the distortions at 10 mm/s, the deformation data was not included in the presented sets. However, the 10 mm/s data for contact-line angle was admitted since it did not rely on using the same reference surface, whereas deformation comparison did.

2.4. Measuring the Surface

Deformation profiles were generated by manually selecting the hydrogel surface through color distinction at the interface of the hydrogel and water. The stitched probe-centered composite image was channel separated to produce a green channel image, corresponding to the hydrogel, and a red channel image, corresponding to the water submerging the hydrogel. Deformation profiles using the individual color channels as well as the combined channel image were used as three deformation data sets. Along a constant Δx, the z-position of the deformed profile was averaged using the three data sets. This average value of z-position of the deformed surface along each Δx was then used to plot the true surface profile (Fig. 3b). The standard deviation between the three data sets is shown as the error for the measurements in Figs. 4 and 5.

To measure the contact distance and contact-line angle, a probe silhouette was overlaid on the deformation profile and the point of deviation of the deformation profile from this probe silhouette is defined as the contact distance. Since the stitched images are probe-centered, and the radius of curvature and size of the probe are known, a probe silhouette was overlaid such that the apex of the probe and the apex of the deformation profile were aligned. The points at which the hydrogel surface and probe join and deviate are defined as the inlet and exit contact distance, respectively. The inlet and exit contact points were selected by inspection. Once these contact points were determined, deformation profile data points ± 250 μm from the contact points were selected and averaged – the standard deviation of these points are shown as the error in Fig. 6. The contact-line angle is then determined by finding the angle between these two points with respect to the horizontal (Fig. 6a).

2.5. Rheology

Rheological measurements were performed on an Anton Paar MCR 702 TwinDrive rheometer using a 25 mm roughened upper plate and a stationary 25 mm roughened lower plate. Rheological samples were prepared at 3.75% pAAm as previously described and cast directly between the upper and lower plates with a working gap of 500 μm. Oscillatory frequency sweeps were performed from 0.1 Hz to 30 Hz at 0.1% strain. Given the torque resolution of the MCR 702 rheometer (0.5 nNm), we determine the minimum shear modulus obtainable under these test conditions to be 0.2 Pa, which is less than the lowest moduli reported here.

3. Results and Discussion

The motivation of this study was to quantitatively measure *in situ* deformations of hydrogels during steady sliding experiments over a wide range of sliding speeds. The scanning speed of the available confocal microscope was too slow to follow high-speed deformations *in situ*. For example, at sliding speeds of 100 mm/s and a contact radius of approximately 1 mm, the deformation through the contact would take place over 20 ms. Therefore, the approach was to perform relatively

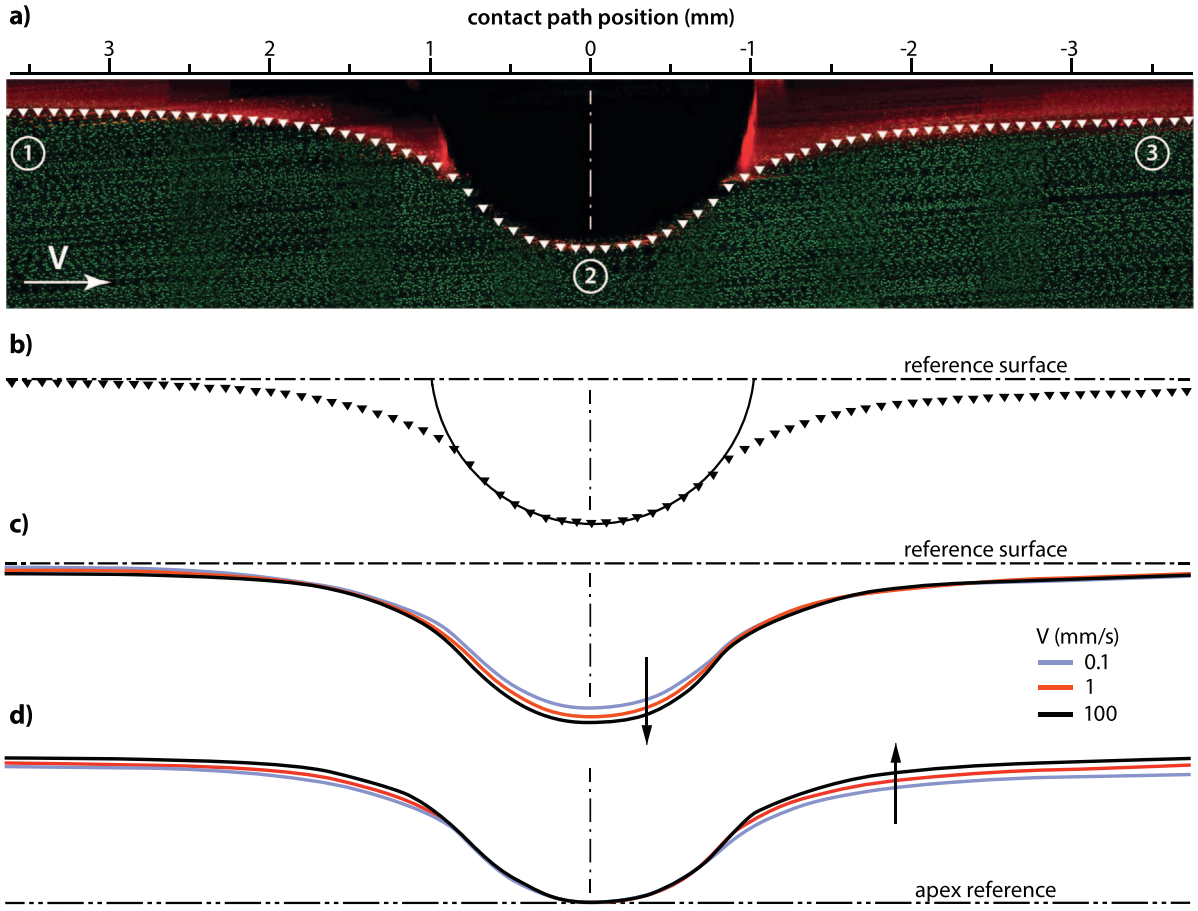

Fig. 3. (a) A composite image of the dynamic deformation of a 10 mm thick 3.75 wt% pAAm hydrogel disk (elastic modulus ~ 500 Pa) under 1 mN of normal force at 0.1 mm/s sliding speed. The green area corresponds to the hydrogel; the red area, the water above the gel; and the black area, the glass probe. The surface profile is determined and marked in white triangles. The inlet region, apex, and exit region are marked as 1, 2 and 3, respectively. The apex of the probe is centered along the x-axis at zero, the inlet region is in the positive direction on the x-axis, and the exit region is negative on the x-axis. (b) Profile data points for 0.1 mm/s are plotted using the unindented surface as a reference. Deformation asymmetries across the probe (solid black semi-circle) are apparent when comparing inlet to exit. (c) An overlay of surface profiles for the three sliding speeds using the unindented hydrogel surface as a reference. Three distinct regions of deformation are observed: (1) inlet deformation changing with sliding speed; (2) probe indentation depth increasing with sliding speed; (3) exit deformation remaining relatively consistent across speeds. (d) Surface profiles overlaid setting the apex of the probe for each deformation field as the reference. Across the profile, it is observed that as speed increases, total vertical deformation increases. (For interpretation of the references to color in this figure legend, the reader is referred to the web version of this article.)

slow confocal scans through a dynamically stable deformation field. Essentially, the probe was held stationary and at equilibrium with a dynamically deforming substrate that was initially flat over the entire testing region, and carefully aligned to be perpendicular with the loading and imaging axes (which were parallel with one another). The result was a dynamic equilibrium of the contact deformation at steady state relative to the stationary spherical probe.

Following the approach outlined in the methods, the hydrogel countersurface deformation was revealed by integrating all of the green fluorescence signal measured during the slow confocal scans. The resulting deformation field was constructed by compositing multiple confocal scans over a range approximately ± 3 contact radii from the probe apex. All testing was performed fully submerged, and the water above the gel was loaded with red fluorescent microbeads that were largely excluded from the contact and revealed the impermeable polished glass sphere through this exclusion. The uncertainty in detecting the surface during sliding was 2.5 μm when imaged through a 10 × objective. The run-out was measured by the deflection of the cantilever over the entire range of sliding was better than 350 nm, which gives ± 50 μN of variation in normal force during these experiments. Digital image analysis was used to measure the surface of the hydrogel during sliding at discrete speeds and loads, as shown in Fig. 3b. The reference surface, shown as a dashed line in Fig. 3b and c, was measured prior to loading and represents the average undeformed surface over the entire range. Fig. 3d shows the measured surface deformation profiles from the reference of the apex of the hemispherical probe (*i.e.* aligned to a fixed reference of the probe).

The deformed surface shape generally followed the expected profile for a Hertzian contact [19,20]; this was particularly true at the slowest sliding speeds. The validity of Hertz was consistent with the symmetric deformation profiles observed by Schulze et al. for hydrogels under quasi-static indentation [21]. Under frictional sliding conditions the deformation field was not guaranteed to be symmetric. As this study finds, the deformation was speed-dependent. Fig. 4 shows the deformation at three distinct locations: (1) inlet, + 3.5 mm in front of the sphere apex; (2) apex of the spherical probe; (3) exit, − 3.5 mm behind the sphere apex. The depth of contact actually increased with increasing speed, although the normal load remained steady at 1 mN (± 50 μN). In the wake of contact at a location of − 3.5 mm, the deformation appeared to be independent of sliding speed over the range of speeds tested, which spanned recovery times of 35 ms to 35 s; however, for the inlet conditions, the recovery was found to be speed-dependent, and considering the circumferential distance traveled, had recovery times from roughly 520 ms to 520 s. This time-dependent recovery from deformation (shown in Fig. 4 at the inlet and exit locations) was consistent with the hypothesis of viscoelastic recovery, and this was one of the

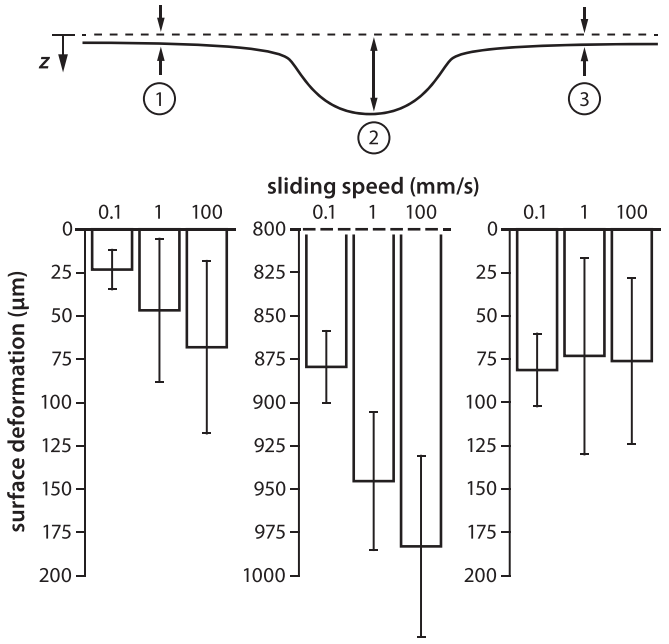

Fig. 4. Deformation of the hydrogel surface with respect to the unindented surface. Inlet region (1) is measured at x = +3.5 mm; apex region (2) is measured at x = 0 mm; exit region (3) is measured at x = −3.5 mm. Inlet deformations increase with speed. Indentation depth increases with speed. Exit region deformations do not appear to change through the speeds tested. Comparing inlet to exit: as sliding speed increases, the elevation of the inlet and exit tend toward similar values. All graphs use the same y-axis scale of 200 μm (note that the graph of apex deformation begins at 800 μm, but uses a 200 μm scale). Error bars represent the standard deviation of surface deformation measurements at positions measured.

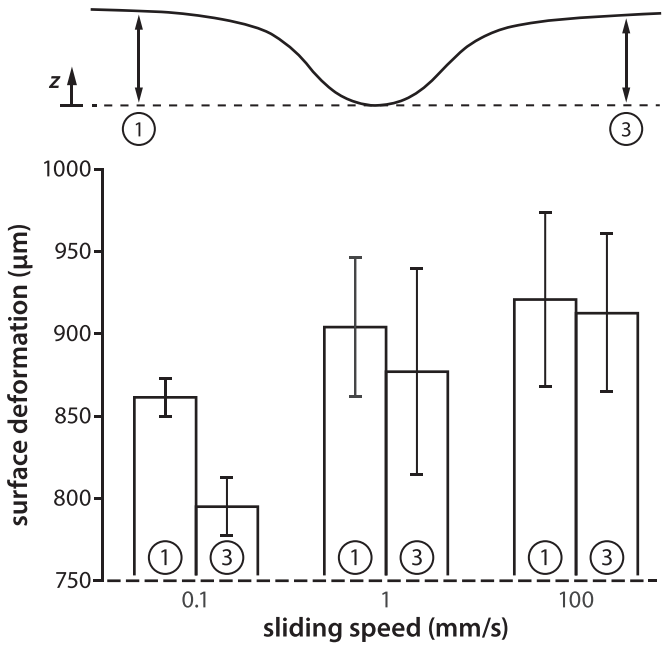

Fig. 5. Surface deformations with respect to apex of the probe. Inlet region and exit region deformation measured at x = +3.5 mm and −3.5 mm respectively. Asymmetries between deformations at the inlet and exit are observed. As sliding speed increases, the surface deformation at the inlet and exit converge, indicating a persistently deformed contact path developing at the inlet with increasing indentation frequency. Additionally, as sliding speed increases, total vertical deformation increases. Error bars represent the standard deviations of surface deformation measurements at the position measured.

expected behaviors for a viscoelastic material. This time-dependent recovery could also be observed if these data were plotted according to deformation from the apex of the probe, as shown in Fig. 5. The inlet and exit regions, (1) and (3) respectively, showed the greatest difference in surface deformation at the lowest sliding speed (0.1 mm/s: 35 s to 520 s) and the least difference at the highest speed (100 mm/s: 35 ms to 520 ms).

Particle exclusion microscopy enabled direct observations of probe-gel contact initiation and separation [22]. These points of contact were found through the divergence of the known spherical geometry of the probe and the observed deformation field of the hydrogel. Measuring the contact distance, defined here as the distance from the centerline of the probe to the initiation of contact (inlet) to the separation of contact (exit), revealed the rate-dependent contact geometry. Fig. 6a shows a contact schematic outlining the local contact geometry with the associated nomenclature. Fig. 6b gives the inlet (s_i) and exit (s_e) distances as a function of sliding speed where the inlet contact distance is shown to monotonically increase with increasing speed, while the exit contact distance is shown to be constant within experimental uncertainties. Connecting a line between the inlet and exit contact points was defined as a contact-line, and drawing a vector normal to this line was the likely axis of the center of pressure. Because the center of pressure axis was no longer parallel with the loading axis, a contact-line angle, α, was measured - plotted in Fig. 6c. The component of force antiparallel to the sliding direction was therefore proportional to the tangent of the contact-line angle, tan(α), which is plotted in Fig. 6d. The relationship between friction coefficient and the tangent of the contact-line angle suggests that the increase in friction coefficient *versus* sliding speed was driven by this contact asymmetry.

Contact asymmetry contributes to the measured friction force. The observed differences between front and back contact distances indicated that the rear of the contact patch did not support as much load as the front. This difference in load support increased with increasing speed, which is consistent with a viscoelastic process in which the recovery rate is outpaced by the separation rate between the sphere and countersurface; the result is a shift of load support preferentially to the front of the contact [1]. A skewed pressure profile was previously reported using finite element analysis of poro-viscoelastic hydrogels [23]. The asymmetric pressure profiles had a component of force in the friction direction, and the resulting friction coefficient was therefore a combination of the interfacial friction and the viscoelasticity of the hydrogel. Interfacial friction was likely low and relatively speed-independent, even under conditions of soft-elastohydrodynamic lubrication as predicted by Hamrock and Dowson. At 100 mm/s, calculations of the minimum fluid film separation were ~5.7 μm [24] resulting in a fluid shear stress of ~15.5 Pa, and a corresponding contribution to friction of μ = 0.03. At all speeds, there was evidence of the red fluorospheres within the contact, but the uncertainties prevent conclusive measurements of the existence of fluid films within the contact.

To experimentally test whether these asymmetric deformation and contact profiles arise from internal viscous stresses in the relaxing hydrogel, low-amplitude oscillatory shear rheology was performed on hydrogel samples cast between parallel roughened plates (see Materials and Methods). The measured $G'(\omega)$ was approximately 600 Pa and was nearly frequency independent over the entire tested range (0.1 Hz to 30 Hz). By contrast, $G''(\omega)$ exhibited a weak frequency dependence at low frequencies, scaling like $\omega^{1/2}$, then rose rapidly, approaching $G'(\omega)$ at higher frequencies (Fig. 7a). By plotting $G''(\omega)/\omega^{1/2}$, the frequency at which $G''(\omega)$ begins to strongly rise was identified, finding the change occurred in the 2–6 Hz range (Fig. 7b). With a shear amplitude of 0.1%, this corresponds to shear-rate amplitudes of 0.01 to 0.04 s^{-1}. To check whether these shear-rates are comparable to those that occurred in the tribological sliding tests, the maximum shear strain under the indented sample was approximated to be d/a, where d is the maximum indentation depth and a is the contact half-width. Since this type of hydrogel is well described by the Hertz model, d/a can be re-written as $a/$

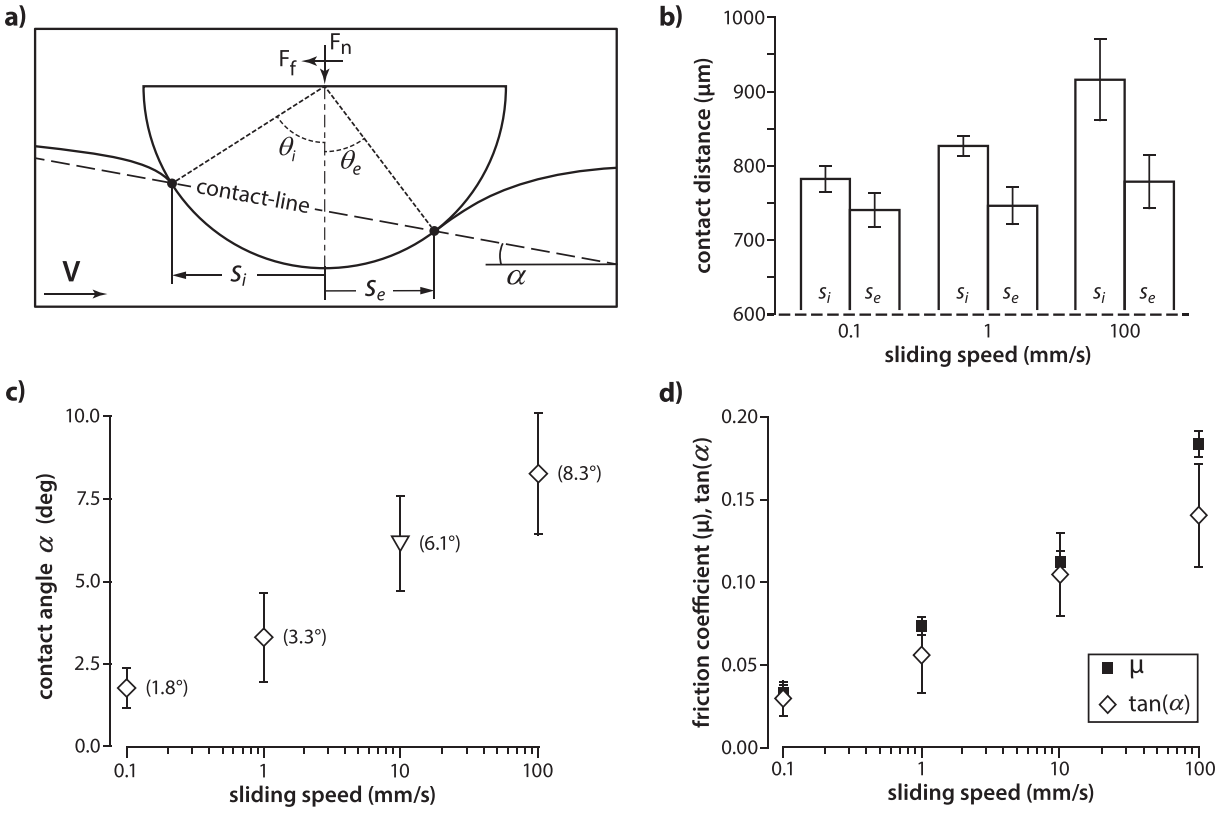

Fig. 6. Contact asymmetry possibly linked to viscoelasticity. (a) A schematic of the sliding contact geometry between a hemispherical glass probe loaded against a hydrogel sheet. Measuring from the probe centerline to the inlet-most and exit-most hydrogel-probe contact points results in the contact distance dimensions s_i and s_e. Drawing a line from the inlet-most contact point to the exit-most contact point creates the contact-line; the angle associated with this contact-line we call contact-line angle α. (b) Inlet and exit contact distances for 0.1, 1, and 100 mm/s were measured from the apex of the probe. Contact distance increases with sliding speed for both the inlet and exit. The contact distance at the inlet rises significantly with sliding speed. With increasing speed, the difference between the inlet and exit contact distance rises. (c) Contact-line angle plotted as a function of sliding speed. It is clear that as the sliding speed increases, so too does the contact-line angle from inlet to exit. The contact-line angle for 10 mm/s (white triangle) was later measured with a different pAAm sample made from the same precursor solution and tested under identical experimental conditions. (d) The coefficient of friction and tangent of contact-line angle α are plotted as a function of sliding speed. The similarity between the tangent of the contact-line angle and the friction coefficient suggests that the increase in friction is highly dependent on the contact-line angle, which may be due to the viscoelasticity of the hydrogel.

R, where R is the radius of curvature of the indenting probe. Thus, the shear rate is approximated to be the first time derivative of a/R. A point just outside of contact moves at the sliding speed, v_{slide}, by the horizontal distance, a, to reach the apex of deformation, so the shear rate is approximately v_{slide} / R. Even at the lowest speed, v_{slide} = 0.1 mm/s, contact asymmetry was observed. With a 1 mm radius of curvature probe, this speed corresponds to a hydrogel shear rate of about 0.1 s^{-1}, larger than the shear rate at which $G''(\omega)$ began to strongly increase in rheological testing. A shear rate of 0.1 s^{-1} corresponds to about 16 Hz, where $G''(\omega)$ approaches $G'(\omega)$ and viscous stresses become comparable to elastic stresses.

Recently, viscoelastic responses of hydrogel deformation and recovery have been observed by performing oscillatory indentation measurements [25]. Our results may reflect the same effects, demonstrating that viscous shear stresses limit the relaxation of hydrogels under sliding, creating contact asymmetry that increases with increasing sliding speed. Such a mechanism does not require fluid exudation or changing polymer concentration under the contact. Recently, indentation studies of pAAm hydrogels showed that water is not driven out of loaded hydrogels when the applied pressure is less than the polymer osmotic pressure [21]. In semi-dilute hydrogels made from flexible polymers, the osmotic pressure is essentially given by the elastic modulus [11]. In the sliding tests here, the maximum applied pressure is 450 Pa, which is slightly below the measured elastic modulus. Thus, contact and deformation asymmetry that determines the measured friction force may arise largely from the sample shear moduli. Deeper investigation into the relative contributions of different potential dissipation mechanisms is required to determine which dominates here. For example, fluid exudation under contact pressure [26] has been considered, and multiple modes of solvent diffusion and polymer chain relaxation were found by Briscoe et al. [27]. However, asymmetric deformation would be expected for all hydrogels regardless of modulus or indenter size. If the elastic modulus were increased, the contribution to deformation by viscoelastic component would be dominated by elastic deformation so the profile asymmetry would attenuate. As indenter size is increased, the resulting asymmetry would again be attenuated as a larger indenter radius equates to lower strain rates, and therefore lower contribution from the rate-dependent viscoelastic component.

There exists potential future work in the development of a dynamic contact model for hydrogels and other biphasic soft materials. Development of this model may require thorough characterization of the individual contributions of mesh size, solvent viscosity, strain rate, contact pressure, and even temperature on the deformation geometry. Furthermore, confocal microscopy enables full-field observations of contact profiles, both local and far-field, in all directions. While measurements in this manuscript were conducted only along the sliding direction, future experiments could include measurements of deformation perpendicular to the sliding direction, which may provide further insights into the geometry of the contact area during sliding.

4. Concluding Remarks

A method to perform slow confocal scans through a dynamic

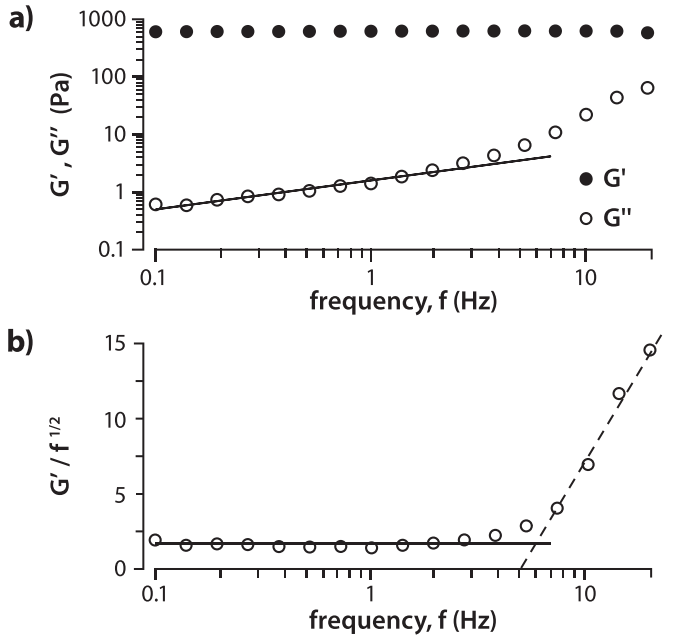

Fig. 7. (a) Low amplitude oscillatory shear rheology on pAAm hydrogels exhibit a frequency-independent elastic modulus, $G'(\omega)$, and a frequency-dependent viscous modulus, $G''(\omega)$. Experiments were performed with roughened parallel plates with a gap of 0.5 mm with a strain-amplitude of 0.1%. A power-law fit to the low frequency range reveals an approximate $\omega^{1/2}$ scaling (solid line is the best fit w^1/2 power law to data within the low frequency range). (b) Plotting $G''(\omega)$ $/\omega^{1/2}$ allows identification of the frequency range where the viscous stresses in the hydrogel begin to dramatically rise.

equilibrium *in situ* was established. Fluorescent microbeads in the hydrogel and solution were used to produce images of the dynamic contact interface and reveal local and bulk deformations during sliding. An asymmetric contact was measured using a 3.75 wt% polyacrylamide gel, and asymmetric deformation between the inlet and exit increased with increasing sliding speed. Changes in friction with sliding speed correlated with the tangent of the contact-line angle. Rheology measurements confirmed that these gels were viscoelastic in the relevant frequency regimes for these contacts.

Acknowledgements

This work was supported by Alcon Laboratories.

References

[1] E.D. Bonnevie, V.J. Baro, L. Wang, D.L. Burris, In situ studies of cartilage microtribology: roles of speed and contact area, Tribol. Lett. 41 (2011) 83–95, http://dx.doi.org/10.1007/s11249-010-9687-0.
[2] G.A. Ateshian, H. Wang, A. Theoretical Contact, Solution for the frictionless rolling of cylindrical cartilage layers, J. Biomech. 28 (1995) 1341–1355.
[3] V.C. Mow, S.C. Kuei, W.M. Lai, C.G. Armstrong, Biphasic creep and stress relaxation of articular cartilage in compression: theory and experiments, J. Biomech. Eng. 102 (1980) 73–84.
[4] W.C. Hayes, A.J. Bodine, Flow-independent viscoelastic properties of articular cartilage matrix, J. Biomech. 11 (1978) 407–419, http://dx.doi.org/10.1016/0021-9290(78)90075-1.
[5] A.F. Mak, The apparent viscoelastic behavior of articular cartilage—the contributions from the intrinsic matrix viscoelasticity and interstitial fluid flows, J. Biomech. Eng. 108 (1986) 123, http://dx.doi.org/10.1115/1.3138591.
[6] B. Weightman, Tensile fatigue of human articular cartilage, J. Biomech. 9 (1976) 193–200, http://dx.doi.org/10.1016/0021-9290(76)90004-X.
[7] A.C. Dunn, W.G. Sawyer, T.E. Angelini, Gemini interfaces in aqueous lubrication with hydrogels, Tribol. Lett. 54 (2014) 59–66, http://dx.doi.org/10.1007/s11249-014-0308-1.
[8] A.A. Pitenis, J.M. Urueña, K.D. Schulze, R.M. Nixon, A.C. Dunn, B.A. Krick, W.G. Sawyer, T.E. Angelini, G. Sawyer, T.E. Angelini, Polymer fluctuation lubrication in hydrogel gemini interfaces, Soft Matter 10 (2014) 8955–8962, http://dx.doi.org/10.1039/C4SM01728E.
[9] J.M. Urueña, A.A. Pitenis, R.M. Nixon, K.D. Schulze, T.E. Angelini, W.G. Sawyer, Mesh size control of polymer fluctuation lubrication in Gemini hydrogels, Biotribology 1–2 (2015) 24–29, http://dx.doi.org/10.1016/j.biotri.2015.03.001.
[10] A.A. Pitenis, J. Manuel Urueña, A.C. Cooper, T.E. Angelini, W.G. Sawyer, Superlubricity in Gemini hydrogels, J. Tribol. 138 (2016) 42103, http://dx.doi.org/10.1115/1.4032890.
[11] P.G. De Gennes, Scaling Concepts in Polymer Physics, Cornell University Press, 1979.
[12] E.D. Bonnevie, V.J. Baro, L. Wang, D.L. Burris, Fluid load support during localized indentation of cartilage with a spherical probe, J. Biomech. 45 (2012) 1036–1041, http://dx.doi.org/10.1016/j.jbiomech.2011.12.019.
[13] S. Kusche, Frictional force between a rotationally symmetric indenter and a viscoelastic half-space, ZAMM-J. Appl. Math. Mech. 97 (2017) 226–239, http://dx.doi.org/10.1002/zamm.201500169.
[14] M. Barquins, R. Courtel, Rubber friction and the rheology of viscoelastic contact, Wear 32 (1975) 133–150, http://dx.doi.org/10.1016/0043-1648(75)90263-X.
[15] K.D. Schulze, A.I. Bennett, K.G. Rowe, W.G. Sawyer, L'Escargot Rapide: soft contacts at high speeds, Tribol. Lett. 55 (2014) 65–68, http://dx.doi.org/10.1007/s11249-014-0332-1.
[16] B.A. Krick, J.R. Vail, B.N.J. Persson, W.G. Sawyer, Optical in situ micro tribometer for analysis of real contact area for contact mechanics, adhesion, and sliding experiments, Tribol. Lett. 45 (2012) 185–194, http://dx.doi.org/10.1007/s11249-011-9870-y.
[17] B.N.J. Persson, N. Prodanov, B.A. Krick, N. Rodriguez, N. Mulakaluri, W.G. Sawyer, P. Mangiagalli, Elastic contact mechanics: percolation of the contact area and fluid squeeze-out, Eur. Phys. J. 35 (2012) 5, , http://dx.doi.org/10.1140/epje/i2012-12005-2.
[18] B.A. Krick, W.G. Sawyer, A little analysis of errors in friction for small wear tracks, Tribol. Lett. 39 (2010) 221–222, http://dx.doi.org/10.1007/s11249-010-9605-5.
[19] H. Hertz, Über die Berührung fester elastischer Körper, J. Für Die Reine Angew. Math. 92 (1882) 156–171.
[20] K.L. Johnson, Contact Mechanics, Cambridge University Press, Cambridge, 1985.
[21] K.D. Schulze, S.M. Hart, S.L. Marshall, C.S. O'Bryan, J.M. Urueña, A.A. Pitenis, W.G. Sawyer, T.E. Angelini, Polymer osmotic pressure in hydrogel contact mechanics, Biotribology (2017), http://dx.doi.org/10.1016/j.biotri.2017.03.004 (In Press).
[22] K.D. Schulze, A.I. Bennett, S. Marshall, K.G. Rowe, A.C. Dunn, Real area of contact in a soft transparent interface by particle exclusion microscopy, J. Tribol. 138 (2016) 41404, , http://dx.doi.org/10.1115/1.4032822.
[23] M.M. Blum, T.C. Ovaert, Experimental and numerical tribological studies of a boundary lubricant functionalized poro-viscoelastic PVA hydrogel in normal contact and sliding, J. Mech. Behav. Biomed. Mater. 14 (2012) 248–258, http://dx.doi.org/10.1016/j.jmbbm.2012.06.009.
[24] B.J. Hamrock, D. Dowson, Elastohydrodynamic lubrication of elliptical contacts for materials of low elastic modulus I—fully flooded conjunction, J. Lubr. Technol. 100 (1978) 236, http://dx.doi.org/10.1115/1.3453152.
[25] P.C. Nalam, N.N. Gosvami, M.A. Caporizzo, R.J. Composto, R.W. Carpick, Nano-rheology of hydrogels using direct drive force modulation atomic force microscopy, Soft Matter 11 (2015) 8165–8178, http://dx.doi.org/10.1039/C5SM01143D.
[26] X. Zhao, N. Huebsch, D.J. Mooney, Z. Suo, Stress-relaxation behavior in gels with ionic and covalent crosslinks, J. Appl. Phys. 107 (2010) 63509, , http://dx.doi.org/10.1063/1.3343265.
[27] B.J. Briscoe, L. Fiori, E. Pelillo, Nano-indentation of polymeric surfaces, J. Phys. D. Appl. Phys. 31 (1998) 2395–2405, http://dx.doi.org/10.1088/0022-3727/31/19/006.
[28] A.C. Rennie, P.L. Dickrell, W.G. Sawyer, Friction coefficient of soft contact lenses: measurements and modeling, Tribol. Lett. 18 (2005) 499–504, http://dx.doi.org/10.1007/s11249-005-3610-0.
[29] J. Schindelin, I. Arganda-Carreras, E. Frise, et al., Fiji: an open-source platform for biological-image analysis, Nature methods 9 (7) (2012) 676–682, http://dx.doi.org/10.1038/nmeth.2019 (PMID 22743772, (on Google Scholar)).